Journal of Ovonic Research Vol. 17, No. 5, September - October 2021, p. 429 - 435

Synthesis and characterization of carbon nanotubes incorporated with MgO nanoparticles

M. E. Ali[a], A. A. Alfaki[a], A. S. Mohammed[b], H. H. Abuelhassan[b], A. A. Qurtam[c], Kh. M. Haroun[d], M. H. Eisa[a,e,*]
[a]*Physics Department, College of Science, Sudan University of Science and Technology, Khartoum 11113, Sudan*
[b]*Physics Department, Faculty of Science, Al-Neenlen University, Khartoum, Sudan*
[c]*Department of Biology, College of Sciences, Imam Mohammad Ibn Saud Islamic University (IMSIU), Riyadh 11623, Saudi Arabia*
[d]*Physics Department, Faculty of Education, Al-Zaiem Al-Azhari University, Omdurman, Sudan*
[e]*Department of Physics, College of Sciences, Imam Mohammad Ibn Saud Islamic University (IMSIU), Riyadh 11623, Saudi Arabia*

For the replacement of industrial materials that are scarce and very expensive, new alternative substances were produced by synthesizing nano materials. Chemical vapor deposition (CVD) method was used to synthesize two types of carbon nanotubes (CNTs) from soot carbon nanotubes [soot CNTs] and coal carbon nanotubes [coal CNTs] in this study. The soot and coal CNTs samples were incorporated with molar concentrations *0.1, 0.3, 0.5, 0.7 and 0.9) of MgO. Fourier Transform Infra-Red Spectroscopy (FTIR) and X-ray Diffraction (XRD) were used to characterize the soot (MgO) and coal (MgO) CNTs samples. CNTs were formed successfully, according to the results of the FT-IR technique. The results of the XRD of the d-spacing, crystals size and density of the magnesium oxide (MgO) integrated into (soot and coal CNTs) or [soot (MgO) and coal (MgO)] CNTs samples were calculated. The impact of the ratios of MgO on CNTs samples' structural properties was calculated. The phases of MgO and its crystalline structure are shown by the XRD method. The study method and results are analyzed in detail.

(Received May 22, 2021; Accepted September 18, 2021)

Keywords: Soot, Coal, CNTs, MgO, D-spacing, Crystal size, CVD

1. Introduction

Nanocomposites of carbon nanotubes (CNT) and nanoparticles (NPs) in one discrete structure enable to combine the unique physical and chemical properties. These two kinds of materials with the unique properties, leading to novel and prospective applications [1]. In the literature great attention has been given to carbon nanotubes (CNTs) [1]. CNTs have special physical, biological and chemical activities [2, 3]. They are utilized for various purposes like solar cell, purification systems, fuel cells, as separation membranes, filters, displays, clothes, sensors, biomedical industry, for hydrogen storage and as a super capacitor [4-8]. The first reports on the biological application of CNTs were published [9,10].

Nanoparticles are classified into two main forms: Multi-walled CNTs (MWCNTs), with diameters between 10nm to 50nm and a single single-walled CNTs (SWCNTs), with diameters between 0.6nm and 3nm [1]. MWNTs have high physical, mechanical, and electrical activities. MWCNTs are weakly bounded by Van der Waals interactions in a tree ring-like structure. SWCNTs consist of a roll of graphene sheet used in forming a cylinder; while MWCNTs are made of multiple rolls of cylinder [8]. Through arc discharge, Mechano-thermal, laser ablation, electrolysis, flame and CVD, CNTs were synthesized in large amounts [11, 12]. CVD was

---

[*] Corresponding author: mheisas@hotmail.com

regarded as the most suitable and cheap technique for growing different types of CNTs under mild environment [13]. CNTs have been produced by different sources of carbon. Hydrocarbon precursor is needed to produce CNTs using CVD method. Methane and acetylene are the commonly used hydrocarbon [14]. Carbon monoxide, soot and coal are other sources of carbon used to produce CNT [15].

It is difficult to prepare uniform samples of filled nanotubes. The surface of CNT cannot attach to metal precursors due to its chemically 'inert' and hydrophobic nature [16]. Thus, it is necessary to modify its surface to establish efficient tube-matrix contacts. The wide distribution of diverse functional groups like hydroxyl, carboxyl, and carbonyl on the surface of CNT can offer active sites for metal ions to attach [17]. Magnesium oxide (MgO) is usually considered as a potential high-surface-area material of CNTs. Nanoscale magnesium oxide has special physical and chemical activities due to its structure [17]. A lot of new techniques that can be used to prepare nano-sized MgO particles [18,19] have been reported in literature.

Nonetheless, there is need to examine the many parameters that influence their production qualities and yields. There are more areas to research on the synthesis of CNTs; and it can open way for the production of value-added products like carbon nanotubes. It is urgently needed to look for an eco-friendly and effective way to handle the organic contaminants in wastewater. Thus, it is necessary to produce carbon nanotube–magnesium oxide composite that is efficient. The production and characterization of CNTs and MgO composites is necessary. Herein, two materials of soot and coal were utilized to uniformly cover CNTs with various ratios of MgO nanoparticles. FTIR and XRD techniques were used to characterize the structure of CNTs and MgO/CNT samples.

2. Materials and methods

2.1. Preparation of Sample

With potassium chlorate ($KClO_3$), nitric acid (HNO_3) and sulfuric acids (H_2SO_4), soot and coal were used to prepare CNTs. First, 5.0g of graphite (soot or coal) was gradually added to sulfuric acid (50mℓ) and fuming nitric acid (25mℓ) mixture and left for 30 minutes. The mixture was cooled down in an ice bath to 5°C. 25.0g of potassium chlorate was gradually added to the mixture and stirred for 30 minutes. When potassium chlorate was added to the solution, there was great heat, thus there is need to be careful at this stage to smear out temperature effect. The mixture was heated up to 70°C for 24 hours and left in the air for 3 days. Most of the graphite were precipitated to the bottom but some carbons that reacted were floating. The floating carbon materials were transferred into deionized water (1ℓ). After being stirred for 1 hour, the solution was filtrated and the sample was dried.

The soot (MgO) and coal (MgO) CNTs samples were named soot $_{0.5}$ $(MgO)_{0.0}$, soot $_{0.5}$ $(MgO)_{0.1}$, soot $_{0.5}$ $(MgO)_{0.3}$, soot $_{0.5}$ $(MgO)_{0.5}$, soot $_{0.5}$ $(MgO)_{0.7}$, soot $_{0.5}$ $(MgO)_{0.9}$, coal $_{0.5}$ $(MgO)_{0.0}$, coal $_{0.5}$ $(MgO)_{0.1}$, coal $_{0.5}$ $(MgO)_{0.3}$, coal $_{0.5}$ $(MgO)_{0.5}$, coal $_{0.5}$ $(MgO)_{0.7}$, and coal $_{0.5}$ $(MgO)_{0.9}$, respectively.

3. Characterization

The vibrational and rotational movements of molecules were analyzed using the FTIR method. Whether functional groups were present or not was detected using Fourier transform infrared spectrum. 14000–10 cm^{-1} range of the electromagnetic spectrum could be analyzed with this method. For confirmation of the presence of CNTs, FTIR spectra were recorded in transmission mode apparatus in the 400 and 4000 cm^{-1} region. XRD is a powerful method used for the determination of the total crystalline structure of nanotubes. The samples were analyzed by XRD on a powder diffractometer (Philips PW1700 X). The XRD used Cu Kα radiation (λ = 0.15418 nm) at a rate of 0.06 oC/second. The XRD pattern was recorded over a 2θ interval of 10° to 50°. The XRD worked at 40 kV and current of 30 mA.

4. Results and discussion

4.1. The FTIR Study of Soot and Coal CNTs doped with MgO

Figures 1 and 2 show the FTIR spectrum of carbon nanotubes of soot and coal CNTs integrated with various ratios of MgO. The properties of soot CNTs incorporated with MgO are seen in Figure 1. A characteristic peak at 3920 cm^{-1} is ascribed to the –C ≡ C–H: C–H bond in the carbon nanotubes. A characteristic peak at 3760 cm^{-1} is due to the O–H bond in the carbon nanotubes. A characteristic peak at 3650 cm^{-1} is ascribed to the O-H bond in the carbon nanotubes. Peak at 3430 cm^{-1} is linked to Phenols and Alcohols (hydrogen-bonded O-H stretch); while the strongest peak situated at 2930 cm^{-1} shows the presence of (C-H stretch) stretching for Alkanes. The characteristic peaks of C = O Stretch are located from 1650 cm^{-1} vibration of carboxylic acids. The peaks located at 1530 cm^{-1} are linked to C=C stretching vibration of aromatic compounds. The strong peak at 1450 cm^{-1} is linked to aromatic rings C-C = C asymmetric stretch vibration, at 1415 cm^{-1} ascribed to C-H bend vibration of alkanes group; the band at 1040cm^{-1} is linked to esters group (C-O stretch) vibration. Peak at 570 cm^{-1} is ascribed to alkyl halides C–Br stretch, while the strongest peak located at 470 cm^{-1} shows the presence of (C-H bend patterns for aromatics) stretching for Meta (MgO) replaced aromatic.

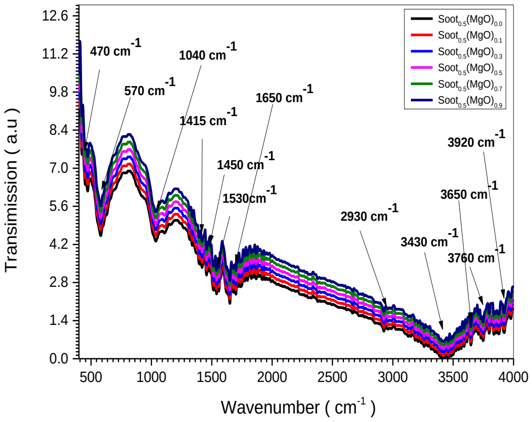

Fig. 1. IR spectra of the soot $_{0.5}$ (MgO)$_{0.0}$, soot $_{0.5}$ (MgO)$_{0.1}$, soot $_{0.5}$ (MgO)$_{0.3}$, soot $_{0.5}$ (MgO)$_{0.5}$, soot $_{0.5}$ (MgO)$_{0.7}$ and soot $_{0.5}$ (MgO)$_{0.9}$

The properties of coal CNTs incorporated with MgO are seen in Figure 2. A characteristic peak at 3850 cm^{-1} is due to the –C ≡ C–H: C–H bond in the carbon nanotubes. A characteristic of peak at 3700 cm^{-1} is ascribed to the O–H bond in vibration of alcohol group of the carbon nanotubes. A characteristic peak at 3380 cm^{-1} is due to the phenols and alcohols O-H bond in the carbon nanotubes. Peak at 3120 cm^{-1} is linked to amines primary N - H stretch, while the strongest peak at 1630 cm^{-1} shows the presence of C = C stretch, stretching for Alkenes. The characteristic peaks of C-H stretch are located from 1400 cm^{-1} vibration of aromatic. The peaks at 1100 cm^{-1} are linked to C-O stretch vibration of esters compounds. The strongest peak at 620 cm^{-1} is ascribed to alkyl halides C–Br stretch vibration.

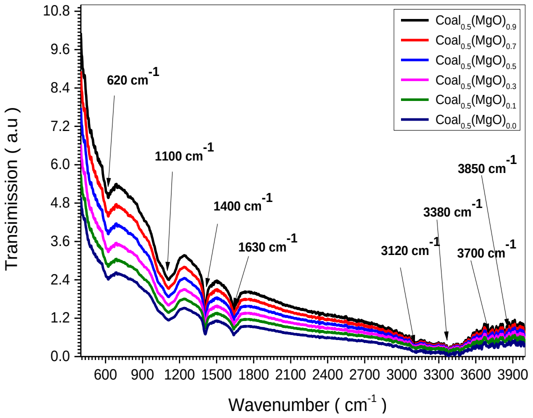

Fig. 2. IR spectra of the coal $_{0.5}$ (MgO)$_{0.0}$, coal $_{0.5}$ (MgO)$_{0.1}$, coal $_{0.5}$ (MgO)$_{0.3}$, coal $_{0.5}$ (MgO)$_{0.5}$, coal $_{0.5}$ (MgO)$_{0.7}$, and coal $_{0.5}$ (MgO)$_{0.9}$.

4.2. XRD Study on Soot and Coal CNTs incorporated with MgO

Figures 3 and 4 show the XRD spectra of CNTs before and after being incorporated with various ratios of MgO. The XRD spectra of the soot (MgO) and coal (MgO) CNTs samples are conducted to identify the crystal structure, size and phase composition. In Figure 3, the soot $_{0.5}$ (Mg O) $_{0.0}$ sample has molar crystallites with (Monoclinic–primitive) crystal structure at (a=21.41, b=7.2792 and c=9.5221) and ($\alpha = 90^{O}$, $\beta = 97.945^{O}$ and $\gamma = 90^{O}$). The soot $_{0.5}$ (Mg O) $_{0.1}$ sample has molar crystallites with (Hexagonal–primitive) crystal structure at (a = b= 2.456 and c = 20.088) and ($\alpha = \beta = 90^{O}$ and $\gamma = 120^{O}$). The soot $_{0.5}$ (Mg O) $_{0.3}$ sample has molar crystallites with (Orthorhombic–primitive) crystal structure at (a = 12.372, b=37.1 and c = 3.954) and ($\alpha = \beta = \gamma = 90^{O}$). The soot $_{0.5}$ (MgO) $_{0.5}$ sample has molar crystallites with (Monoclinic–primitive) crystal structure at (a =9.736, b= 8.469 and c = 12.777) and ($\alpha = 90^{O}$, $\beta = 90.56^{O}$ and $\gamma = 90^{O}$). The soot $_{0.5}$ (MgO) $_{0.7}$ sample has molar crystallites with (Monoclinic–primitive) crystal structure (a = 6.9754, b = 12.764 and c = 6.962) and ($\alpha = 91.16^{O}$, $\beta = 90.32^{O}$ and $\gamma = 83.22^{O}$). The soot $_{0.5}$ (MgO) $_{0.9}$ sample has molar crystallites with (Monoclinic–primitive) crystal structure at (a = b = 2.456 and c = 20.088) and ($\alpha = \beta = 90^{O}$ and $\gamma = 120^{O}$).

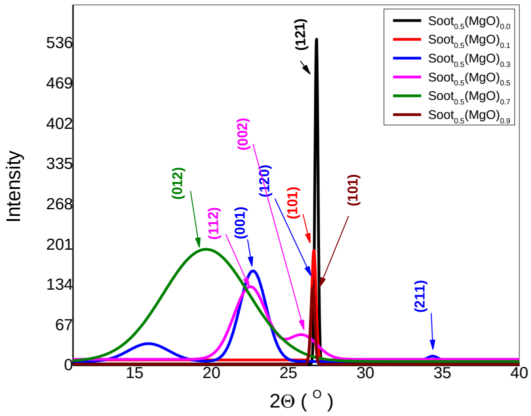

Fig. 3. The XRD spectra of the soot $_{0.5}$ (MgO)$_{0.0}$, soot $_{0.5}$ (MgO)$_{0.1}$, soot $_{0.5}$ (MgO)$_{0.3}$, soot $_{0.5}$ (MgO)$_{0.5}$, soot $_{0.5}$ (MgO)$_{0.7}$ and soot $_{0.5}$ (MgO)$_{0.9}$.

The miller indices of the coal $_{0.5}$ (MgO)$_{0.0}$, coal $_{0.5}$ (MgO)$_{0.1}$, coal $_{0.5}$ (MgO)$_{0.3}$, coal $_{0.5}$ (MgO)$_{0.5}$, coal $_{0.5}$ (MgO)$_{0.7}$, and coal $_{0.5}$ (MgO)$_{0.9}$ are shown in Figure 4. The coal $_{0.5}$ (Mg O) $_{0.0}$ sample has molar crystallites with (Tetragonal–primitive) crystal structure at (a = b = 7.46 and c = 8.61) and ($\alpha = \beta = \gamma = 90^{O}$). The coal $_{0.5}$ (MgO) $_{0.1}$ sample has molar crystallites with (Cubic–primitive) crystal structure at (a = b= c = 4.152) and ($\alpha = \beta = \gamma = 90^{O}$). The coal $_{0.5}$ (MgO) $_{0.3}$

sample has molar crystallites with (Monoclinic –primitive) crystal structure at (a = 7.1986, b = 7.9393 and c = 17.39) and ($\alpha = 90^{O}$, $\beta = 90.6204^{O}$ and $\gamma = 90^{O}$). The coal $_{0.5}$(MgO)$_{0.5}$ sample has molar crystallites with (Hexagonal –primitive) crystal structure at (a = b = 5.39 and c = 46.52 and c = 17.39) and ($\alpha = \beta = 90^{O}$ and $\gamma = 120^{O}$). The coal $_{0.5}$ (MgO)$_{0.7}$ sample has molar crystallites with (Triclinic –primitive) crystal structure at (a = 6.485, b = 6.415 and c = 16.8) and ($\alpha = 90.11^{O}$, $\beta = 95.91^{O}$ and $\gamma = 90.95^{O}$). The coal $_{0.5}$ (Mg O)$_{0.9}$ sample has molar crystallites with (Orthorhombic –primitive) crystal structure at (a = 11.35, b = 24.08 and c = 4.1398) and ($\alpha = \beta = \gamma = 90^{O}$).

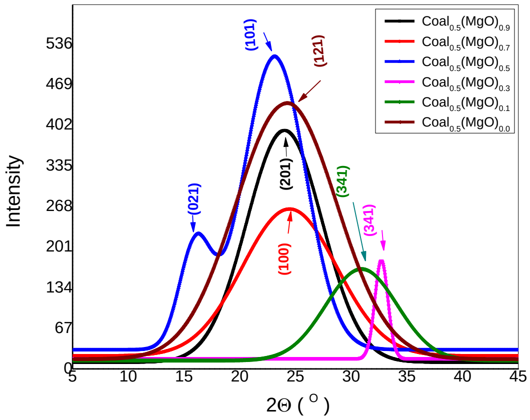

Fig. 4. The XRD spectra of the coal $_{0.5}$ (MgO)$_{0.0}$, coal $_{0.5}$ (MgO)$_{0.1}$, coal $_{0.5}$ (MgO)$_{0.3}$, coal $_{0.5}$ (MgO)$_{0.5}$, coal $_{0.5}$ (MgO)$_{0.7}$, and coal $_{0.5}$ (MgO)$_{0.9}$.

The XRD parameters, crystal size, d-spacing and density of the soot $_{0.5}$ (MgO)$_{0.0}$, soot $_{0.5}$ (MgO)$_{0.1}$, soot $_{0.5}$ (MgO)$_{0.3}$, soot $_{0.5}$ (MgO)$_{0.5}$, soot $_{0.5}$ (MgO)$_{0.7}$ and soot $_{0.5}$ (MgO)$_{0.9}$ CNTs are shown in Table 1. We calculated the crystals size, density and interlayer spacing of the soot (MgO) CNPS samples. The density and d-spacing of the soot (MgO) CNPS reduced with increased molar concentration of MgO. But, the soot (MgO) CNPS' crystal size increased with increased molar concentration of MgO. The d-spacing of the soot (MgO) CNPS dropped from 0.33608 nm to 3.3258 nm with increased molar concentration of MgO. The soot (MgO) CNPS' crystal sizes increased from 07.9nm to 35.6nm with increased molar concentration of MgO. Diffraction peaks were used to calculate each sample's average crystallite size with Debye–Scherrer equation. By adding MgO, the soot CNPS' density dropped from 4.7179 mg.cm^{-3} to 2.8161 mg.cm^{-3}. The findings show that the highest value of the density of soot$_{0.5}$(MgO)$_{0.0}$ is 4.7179 mg.cm^{-3}. The density decreased because the structural defects and/or impurities increased, including the resultant soot and other pollutants from the precursor.

Table 1. The d-spacing, crystal size and density of the soot $_{0.5}$ (MgO)$_{0.0}$, soot $_{0.5}$ `(MgO)$_{0.1}$, soot $_{0.5}$ (MgO)$_{0.3}$, soot $_{0.5}$ (MgO)$_{0.5}$, soot $_{0.5}$ (MgO)$_{0.7}$ and soot $_{0.5}$ (MgO)$_{0.9}$ CNPS.

Samples	**d (A^{0})**	**X$_s$ (nm)**	**δ (mg.cm^{-3})**
Soot$_{0.5}$(MgO)$_{0.0}$	3.3608	07.9	4.7179
Soot$_{0.5}$(MgO)$_{0.1}$	3.3532	08.2	3.7849
Soot$_{0.5}$(MgO)$_{0.3}$	3.3458	08.9	3.6697
Soot$_{0.5}$(MgO)$_{0.5}$	3.3393	19.0	3.2114
Soot$_{0.5}$(MgO)$_{0.7}$	3.3321	32.5	2.9424
Soot$_{0.5}$(MgO)$_{0.9}$	3.3258	35.6	2.8161

The XRD parameters, the d-spacing**,** crystal size and density of the coal $_{0.5}$ $(MgO)_{0.0}$, coal $_{0.5}$ $(MgO)_{0.1}$, coal $_{0.5}$ $(MgO)_{0.3}$, coal $_{0.5}$ $(MgO)_{0.5}$, coal $_{0.5}$ $(MgO)_{0.7}$, and coal $_{0.5}$ $(MgO)_{0.9}$ are shown in Table 2. We calculated the interlayer spacing, crystals size and density of the coal (MgO) samples. The coal (MgO) CNPS' d-spacing and crystal sizes increased with increased molar concentration of MgO. But, the coal (MgO) CNPS' density decreased with increased molar concentration of MgO. The coal (MgO) CNPS' d-spacing increased from 0.34246nm to 0.3676nm with increased molar concentration of MgO. The coal (MgO) CNPS' crystal sizes increased from 47.7nm to 75.1nm with increased molar concentration of MgO. By adding MgO, coal CNPS' density dropped from 6.4267mg. cm^{-3} to 0.1752 $mg.cm^{-3}$.

Table 2. The d-spacing, crystal size and density of the of the coal $_{0.5}$ $(MgO)_{0.0}$, coal $_{0.5}$ $(MgO)_{0.1}$, coal $_{0.5}$ $(MgO)_{0.3}$, coal $_{0.5}$ $(MgO)_{0.5}$, coal $_{0.5}$ $(MgO)_{0.7}$, and coal $_{0.5}$ $(MgO)_{0.9}$.

Samples	*d (A^0)*	*X_s (nm)*	*δ ($mg.cm^{-3}$)*
$coal_{0.5}(MgO)_{0.0}$	3.4246	47.7	6.4267
$coal_{0.5}(MgO)_{0.1}$	3.4685	54.4	4.1522
$coal_{0.5}(MgO)_{0.3}$	3.4876	68.0	3.7849
$coal_{0.5}(MgO)_{0.5}$	3.5394	67.5	3.2114
$coal_{0.5}(MgO)_{0.7}$	3.6399	70.3	2.8746
$coal_{0.5}(MgO)_{0.9}$	3.6760	75.1	0.1752

4. Conclusion

Due to the special physical and chemical properties of carbon nanomaterials a lot of attention has been given to their production and characterization. Coot and coal were compared to synthesize CNTs in order to see the structure and impact of adding MgO onto CNTs. CVD was used to synthesize the soot and coal (MgO) CNTs samples successfully and FTIR and XRD techniques were used to confirm them. The FTIR analysis shows that, the characterization multitasked matching vibration association Alcohols O-H stretch (strong and broad), while there was a small change in the vibration of the following links (alkyl halides C–Br stretch, Esters (C-O Stretch), Aromatic C-H stretch, Alkenes C=C stretch, alcohols O–H stretch and alkynes (terminal) –C ≡ C–H: C–H stretch). But, for the coal (MgO) NP_S, links were missing (meta substituted aromatic C-H bend patterns for aromatics, alkane C-H bend, Aromatic Rings C-C=C Asymmetric Stretch, Carboxylic Acids C=O Stretch, Phenols & Alcohols and Hydrogen-bonded O-H Stretch). The results of XRD show that, the d-spacing and the density of the soot (MgO) NPS decreased with increased molar concentration of MgO. But, the crystals size of the soot (MgO) NPS increased with increased molar concentration of MgO. The results of XRD show that, d-spacing and crystal sizes of the coal (MgO) NPS increased with increased molar concentration of MgO. While, the results of XRD show that, the density of the coal (MgO) NPS decreased with increased molar concentration of MgO.

Acknowledgments

The authors supported privately this research. There is no grant number or funding to declare.

References

[1] S. Iijima, Nature **354**, 56 (1991).
[2] A. Eatemadi, H. Daraee, H. Karimkhanloo, M. Kouhi, N. Zarghami, A. Akbarzadeh,

M. Abasi, Y. Hanifehpour, S. W. Joo, Nanoscale Res Lett. **9**(1), 393 (2014).
[3] R. Kotsilkova, E. Ivanov, D. Bychanok, A. Paddubskaya, M. Demidenko, J. Macutkevic, P. Kuzhir, Composites Science and Technology **106**, 85 (2015).
[4] P. Lva, P. Zhanga, F. Lia, Y. Lia, Y. Fenga, W. Fenga, Synthetic Metals **162**(13–14), 1090 (2012).
[5] X. Wang, Z. Li, W. Xu, S. A. Kulkarni, S. K. Batabyal, S. Zhang, L. H. Wong, Nano Energy **11**, 728 (2015).
[6] W. Su, Y., Zhu, J. Zhang, Y. Liu, Y. Yang, Q. Mao, L. Li, Journal of Alloys and Compounds **669**, 8 (2016).
[7] J. Prasek, J. Drbohlavova, J. Chomoucka, J. Hubalek, O. Jasek, V. Adam, R. Kizek, J. Mater. Chem. **21**, 15872 (2011)
[8] L. Camilli, M. Scarselli, S. Del Gobbo, P. Castrucci, F. Nanni, E. Gautron, S. Lefrant, M. De Crescenzi, Carbon **49**(10), (33072011).
[9] Y. Kong, D. X Cui, C. S Ozkan, H. J. Gao, Syst. (Biomems) **773**, 111 (2003).
[10] Q. Guo, X. T. Shen, Y. Y. Li, S. Q. Xu, CCurr. Med. Sci. **37**, 635 (2017).
[11] C. Laurent, E. Flahaut, A. Peigney, Carbon **48**, 2994 (2010).
[12] B. Bhushan, Springer handbook of nanotechnology. Berlin, Germany: Springer (2004)
[13] A. Szabó, C. Perri, A. Csató, G. Giordano, D. Vuono, J. B. Nagy, Materials **3**(5), 3092 (2010).
[14] D. J. S. Jones, P. Pujadó, Petroleum products and a refinery configuration, (Eds.), Handbook of Petroleum Processing, Netherlands: Springer, 47 (2006).
[15] J. Qiu, Y. An, Z, Zhao, Y. Li, Y. Zhou, Fuel Processing Technology **85**(8-10), 913 (2004).
[16] K. Hernadi, E. Ljubovic, J. W. Seo, L. Forro, Acta Mater **51**, 1447 (2003).
[17] L. Zhao, L. Gao, Carbon **42**, (4232004).
[18] W. Wang, X. Qiao, J. Chen, H. Li, Mater Lett **61**, 3218 (2007).
[19] D. Kumar, V. B. Reddy, B. G. Mishra, R. K. Rana, M. N. Nadagouda, R. S. Varma, Tetrahedron **63**, 3093 (2007).